ERK regulates RhoA activation and tumour cell plasticity by inhibiting GEF-H1 activity

Anne von Thun[1,6], Christian Preisinger[1], Oliver Rath[1], Juliane P. Schwarz[1], Chris Ward[1], Naser Monsefi[4], Javier Rodríguez[4], Amaya Garcia-Munoz[4], Marc Birtwistle[4,5], Willy Bienvenut[1], Kurt Anderson[1], Walter Kolch[1,2,3,4#], Alex von Kriegsheim[1,4,#]

[1] The Beatson Institute for Cancer Research, Glasgow G61 1BD, UK

[2] Conway Institute of Biomolecular & Biomedical Research, University College Dublin, Belfield, Dublin 4, Ireland

[3] School of Medicine and Medical Science, University College Dublin, Belfield, Dublin 4, Ireland

[4] Systems Biology Ireland, University College Dublin, Belfield, Dublin 4, Ireland

[5] Department of Pharmacology and Systems Therapeutics, Icahn School of Medicine at Mount Sinai, New York, NY, 10029, USA

[6] Current address: Molecular Biology Department, Wuerzburg University, Wuerzburg, Germany

[#] to whom correspondence should be directed

Contacts

Alex.von Kriegsheim alex.vonkriegsheim@ucd.ie

Walter Kolch walter.kolch@ucd.ie

Running Title

ERK regulates invasion via GEF-H1

Word count:

Materials and Methods: 1131

Introduction, Results, and Discussion: 4004

Abstract

In certain *Ras* mutant cell lines the inhibition of ERK signalling increases RhoA activity and inhibits cell motility, which was attributed to a decrease in Fra-1 levels. Here, we report a Fra-1 independent augmentation of RhoA signalling during short-term inhibition of ERK signalling. Using mass spectrometry based proteomics we identified the Rho exchange factor GEF-H1 as mediating this effect. ERK binds to GEF-H1 and phosphorylates it on S959 causing inhibition of GEF-H1 activity and a consequent decrease in RhoA activity. Knockdown experiments and expression of a non-phosphorylatable S959A GEF-H1 mutant showed that this site is crucial in regulating cell motility and invasiveness. Thus, we identified GEF-H1 as a critical ERK effector that regulates motility, cell morphology and invasiveness.

Introduction

Locomotion, and thus invasion and metastasis of tumour cells, is controlled by cytoskeletal reorganisations, which are coordinated by the tightly regulated and localised activation of the Rho family GTPases, namely RhoA, Rac and CDC42. Rac and CDC42 are mainly activated at the leading edge, whereas RhoA activity is localised at the rear and front of the moving cell (1-4). In cells randomly migrating on two-dimensional surfaces RhoA activity precedes the formation of a protrusion, whereas Rac1 and CDC42 activity peak shortly afterwards during the retraction phase (1). Further, RhoA and Rac1 activities are inversely related due to mutual negative feedback connections (5, 6).

In three dimensional matrices cell motility has different characteristics than on two dimensional surfaces and involves two distinct modes of invasion. Either cells are elongated and move in a matrix metallo-protease (MMP) dependent mesenchymal fashion, or the cells appear rounded and invade in a RhoA dependent, amoeboid way (7) requiring high Rho-kinase (ROCK) activity. RhoA and ROCK control cellular contractility, thus enabling the invading cell to squeeze through the extracellular matrix without the need to degrade it by secreting MMPs. Cells can switch between amoeboid and mesenchymal invasion (5, 8, 9).

The rapid, spatially restricted and controlled activation/deactivation cycle of Rho family GTPases is regulated by a balance of guanidine exchange factors (GEF) and GTPase activating proteins (GAP). GEFs binding to RhoA release bound GDP, which is replaced by abundant cellular GTP. GTP binding induces a conformational switch that unmasks binding sites for downstream effectors. Termination of Rho signalling is achieved through the binding of GAPs. These proteins associate with small GTPases

and, by creating an active site, dramatically increase their intrinsic GTP hydrolysis activity, thus reverting Rho family member to the inactive GDP bound state. GEF and GAP activity as well as their sub-cellular localisation, is controlled by a multitude of external signalling pathways, including Rho/Rac/CDC42 dependent signalling. This high level of regulation, cross talk and complexity at the GEF/GAP level and the fact that constitutively active GEFs have been identified as oncogenes, is driving extensive research interest in these regulatory proteins (for a review see (10)).

Recently, GEF-H1 (ARHGEF2) was identified as an upstream regulator of leading-edge RhoA activity in migrating cells (11). Depletion of GEF-H1 by siRNA decreased RhoA activity at the leading edge as well as random migration and focal adhesion turnover. As with many GEFs, the regulation of GEF-H1 is complex involving a multitude of phosphorylations on activating and inactivating sites. Different kinases including PAK, Aurora A, Cdk1 and PAR1b (12-15) were shown to inactivate GEF-H1 by phosphorylating inhibitory sites, whereas ERK (16, 17) was reported to phosphorylate Thr678, an activating site. Interestingly, regulation of GEF-H1 activity downstream of ERK appears to be more complex, as inhibition of the MAPK-pathway in unstimulated cells not only enhances RhoA activity but, controversially, increases the phosphorylation of the reported ERK phosphorylation site, Thr678 (18). Further, GEF-H1 is held in an inactive conformation when bound to microtubules. Conversely, microtubule disassembly results in a robust activation of RhoA via GEF-H1 (19).

Here, we show that under growing conditions ERK phosphorylates GEF-H1 on an inhibitory site. Inhibition of ERK signalling with chemical MEK-inhibitors induces RhoA activation in a GEF-H1 dependent manner. Overexpression of an

unphosphorylatable GEF-H1 mutant enhances RhoA activity and blocks cell migration and invasiveness. In addition, preventing ERK inhibition of GEF-H1 induces cells to adopt a rounded morphology, and GEF-H1 downregulation interferes with amoeboid invasion.

Materials and Methods

Cells and reagents. Cells were cultured in DMEM supplemented with 2 mM glutamine and 10% foetal calf serum. Plasmids and siRNA oligonucleotides were transfected with Lipofectamine2000 using the manufacturer's instructions (Invitrogen, UK). eGFP-GEF-H1 was kindly provided by Gary Bokoch (Scripps Institute, La Jolla USA) , and GST-Rhotekin-RBD by Mike Olson (Beatson Institute, Glasgow UK). Rat GEF-H1 was cloned from PC12 cDNA by PCR and subsequently cloned into pcDNA3.1 using the NotI and XbaI cloning sites. Flag-GEF-H1-S959A and Flag-GEF-H1-S959D mutants were made using the Quickchange kit (Stratagene, The Netherlands). Antibodies for ERK1, RhoA, and Fra-1 were from Santa Cruz (Clane, UK); for GEF-H1 and ERK substrate motif (pTP, PXpST) from Cell Signalling (Hitchin, UK), ERK1/2 and phospho-ERK1/2 from Sigma (Gillingham, UK); The 3DA-Luciferase reporter vector and TAT-C3 were a kind gift from Mike Olson (Beatson Institute, Glasgow UK), U0126 was from Promega (UK) PD0325901 from Sigma (UK).

siRNA knockdown. 40 pmol siRNA oligonucleotides were introduced into MDA-MB-231 cells by transfection using HiPerFect (Qiagen) according to the manufacturer's instructions. SMARTpool siRNAs or single siRNAs (Dharmacon, USA) were used to knockdown GEF-H1; a non-targeting siRNA pool (Dharmacon,

USA) was used as control. Oligos: #1 GAAUUAAGAUGGAGUUGCA #2 GUGCGGAGCAGAUGUGUAA

Motility assays. Inverted invasion assays (20), were performed as described previously (21). Cells were allowed to invade towards a gradient of EGF (30 nM) and 10% serum for 3 days. In the case of A375M2 cells the Transwell plugs were coated with a 0.001% solution of fibronectin to facilitate migration through the membrane.

Cell treatment, lysis and immunoprecipitation. Cells were incubated with U0126 (10 μM), PD0325901 (2 μM) or serum-deprived for 18 hours and treated with 20 ng/ml EGF as indicated. Cells were lysed in ice-cold lysis buffer (20 mM HEPES pH7.5, 150 mM NaCl, 1% NP40, 2 mM EDTA) supplemented with protease (1 mM PMSF, 5 μg/ml leupeptin, 2.2 μg/ml aprotinin, 2 mM sodium fluoride) and phosphatase (1 mM sodium vanadate, 1 mM sodium pyrophosphate, 20 mM β-glycerophosphate) inhibitors. Lysates were cleared of debris by centrifugation at 20,000 g for 10 minutes in a benchtop centrifuge. For immunoprecipitation antibodies/Protein A agarose beads (GE Healthcare), anti-FLAG-M2 beads (Sigma, UK) or anti-GFP beads (Chromotek, Germany) were added to the cleared lysates and incubated at 4ºC under end-to-end rotation for 2 hours. Beads were washed 3x with lysis buffer and either eluted with a FLAG-peptide, boiled off in Laemmli buffer or, if the samples were destined for mass spectrometry, were washed twice with lysis buffer devoid of detergents

Phosphopeptide mapping. Flag-GEF-H1 was expressed in HEK293 cells and immunoprecipitated with Flag-antibody. The immunoprecipitate was extensively washed, equilibrated with ERK kinase buffer (150 mM NaCl, 10 mM $MgCl_2$, 20 mM Tris-HCl, 1 mM DTT, 1 mM sodium vanadate, 1 mM sodium pyrophosphate, 20mM

β-glycerophosphate pH 7.5) and incubated with active ERK (Calbiochem, UK), 300μM ATP spiked with 1 μl [^{32}P]-γ-ATP (Invitrogen, UK) for 30 minutes. As control ERK was incubated with the widely used substrate myelin basic protein (MBP). The kinase reactions were separated by SDS-PAGE and in-gel digested with trypsin (22). The peptide mixture was separated by RP-HPLC. The radioactive fractions were split, with one fraction subjected to Edman degradation and the other to MALDI-mass spectrometry (MS). Edman degradation indicated that the major phosphorylation site is located on position 6. MS analysis of the radioactive peptide fraction was performed using a Bruker Ultraflex II TOF in positive ion mode using dihyroxybenzoic acid as matrix. Resulting spectra were manually searched for tryptic peptides with a modification of +80 and either S/T or Y on position 6. **.**

Alternatively, HEK293 or HCT116 cells transfected with GFP-GEF-H1 or vector, incubated for 30 minutes with 10 μM U0126 or DMSO. Immunoprecipitated GEF-H1 was digested on the beads. After washing twice with 300 μL ice cold PBS, beads with bound proteins were eluted in two steps. First, by using 60 μl of eluting buffer I (50 mM Tris-HCl pH 7.5, 2 M Urea and 50 μg/ml Trypsin (modified sequencing grade trypsin, Promega) and incubated while shaking at 27°C for 30 minutes, and secondly by adding two times 25 μl of elution buffer II (50 mM Tris-HCl pH 7.5, 2 M Urea and 1 mM DTT). Both supernatants were combined and incubated overnight at room temperature.

Samples were alkylated (20 μl iodoacetamide, 5 mg/ml, 30 min in dark). Then, the reaction was stopped with 1 μl 100% Trifluoracetic acid (TFA) and 100 μl of the sample was immediately loaded into equilibrated handmade C18 StageTips containing Octadecyl C18 disks (Supelco, Sigma UK). C18 StageTips, spin adaptors and solvents were prepared as described previously (23). Samples were desalted by

using two times 50 µl of 0.1% TFA and eluted with two times 25 µl of 50% AcN and 0.1% TFA solution. Final eluates were combined and concentrated until volume was reduced to 5 µl using a CentriVap Concentrator (Labconco, USA). Samples were diluted to obtain a final volume of 12 µl by adding 0.1% TFA and analysed by MS. The tryptic peptides were analysed on a Thermo Scientific Q-Exactive mass spectrometer connected to an Ultimate Ultra3000 chromatography system incorporating an auto-sampler. 5 µl of the resuspended tryptic peptides were loaded onto a homemade column (100 mm length, 75 mm ID) packed with 1.8 µm RepreosilAQ C18 (Dr Maisch, Germany) and separated by an increasing acetonitrile gradient, using a 40 minute reverse phase gradient at a flow rate of 200 nL/min. The mass spectrometer was operated in positive ion mode with a capillary temperature of 220°C, with a potential of 2000 V applied to the column. Data were acquired with the mass spectrometer operating in automatic data dependent switching mode selecting the 12 most intense ions prior to MS/MS analysis. Mass spectra were analysed by MaxQuant. Label-free quantitation was performed using MaxQuant

RhoA-GTP pulldown assays. Cells were lysed in ice-cold lysis buffer (20 mM HEPES pH7.5, 150 mM NaCl, 1% NP40, 2 mM EDTA) supplemented with protease inhibitors (1 mM PMSF, 5 µg/ml leupeptin, 2.2 µg/ml aprotinin, 2 mM sodium fluoride) and 10 mM $MgCl_2$. Cleared lysates were incubated with 5 µl GST-Rhotekin-beads for 30 min at 4ºC under end-to-end rotation. The beads were washed, boiled in Laemmli buffer and Western blotted. The Western blot bands were quantified using ImageJ. Bar graphs represent RhoA-GTP/input RhoA.

Luciferase assay. HCT116 cells were transfected using Lipofectamine 2000 (Invitrogen, UK) according to the manufacturer's instructions with GEF-H1 plasmids,

3DA-luciferase and a renilla control vector. 48 hours later the cells were lysed and luciferase activity was measured using a dual luciferase kit (Promega) according to the manufacturer's instructions. Firefly luciferase activity was normalised by the renilla output.

Statistical analysis. All experiments were performed in triplicate. Comparisons of RhoA-GTP levels, phosphopeptide concentrations, invasion and morphological changes were assessed using nonparametric Mann-Whitney *U* tests. *P* values of less than 0.05 were considered significant.

Results

MEK inhibition induces RhoGTP independent of Fra-1 expression

Prolonged inhibition of MEK by pharmacological inhibitors was previously shown to increase RhoA activity in several cell lines harbouring mutations that result in a sustained activation of the ERK pathway. This increase in RhoA-GTP was attributed to a decrease of Fra-1 expression caused by inhibition of ERK signalling (24, 25). Reduction of Fra-1 levels increased integrin-mediated RhoA activation and permitted the coupling of RhoA activity to stress-fibre formation.

In order to explore if short-term inhibition of the ERK pathway regulates RhoA activity we used HCT116 cells. HCT116 is a human colorectal adenocarcinoma cell line containing a mutated $KRAS^{G13D}$ allele, which encodes a constitutively activated protein leading to the chronic stimulation of downstream signalling. We showed previously that HCT116 cells respond to prolonged MEK inhibition with a decrease in Fra-1 and an increase in RhoA activity (24). As these observations were obtained after overnight inhibition of MEK, we repeated the experiment at shorter time points in

order to assess if acute inhibition of the ERK pathway suffices to augment RhoA-GTP. RhoA-GTP levels increased within half an hour of MEK inhibition as measured by a Rhotekin-pulldown assay (Fig. 1A). Further RhoA activity peaked after one hour, which coincided with a decrease in general ERK substrate phosphorylation observed using an antibody that recognises the phosphorylated ERK consensus sequence PXpSP (Fig 1B). Fra-1 levels did not decrease within this time period, but only after prolonged MEK inhibition (Fig 1C). These results show that short term inhibition of the ERK pathway is sufficient to increase RhoA activity without downregulation of Fra-1 protein expression. Hence, we concluded that aside from ERK-dependent RhoA regulation via Fra-1, another acute mechanism must exist. As ERK substrate dephosphorylation and RhoA activation peak at the same time, we hypothesised that an upstream activator of RhoA may be inhibited by ERK phosphorylation.

ERK associates with GEF-H1

We previously mapped ERK1 interacting proteins by quantitative mass spectrometry (MS) in PC12 cells (22). Proteins that interacted with ERK1 in an EGF dependent manner included the Rho exchange factor GEF-H1. To confirm the MS data we immunoprecipitated endogenous ERK1 from serum starved and EGF stimulated PC12 cells and examined GEF-H1 association (data available upon request). GEF-H1 bound to ERK1 in an EGF dependent manner. The association increased 5 minutes after EGF addition and started decreasing at 15 minutes. Expressing exogenous Flag-tagged GEF-H1, we verified the dynamics of the interaction with ERK1/2 association peaking at 5 minutes and subsiding to lower levels within 15 minutes (data available upon request), correlating with EGF induced ERK activation dynamics.

Similarly, ERK and GEF-H1 interacted in HCT116 cells in an activation-dependent manner (Fig. 1D). Both proteins could be co-immunoprecipitated in growing cells, and the interaction was disrupted, if MEK and consequently ERK activity were inhibited by U0126, thus confirming the results from PC12 cells.

ERK phosphorylates GEF-H1 on S959

ERK was recently reported to phosphorylate GEF-H1 on T678 and cause its activation (16). By contrast, our results suggested that ERK signalling restricts GEF-H1 activation. Therefore, we determined whether ERK was phosphorylating additional sites on GEF-H1. We introduced eGFP-tagged wild type (wt) GEF-H1 into HEK293 cells and enriched the protein by immunoprecipitation. GEF-H1 can be expressed to high levels in this cell line. Further, expression in a mammalian expression system ensures that the protein is folded correctly. The immunoprecipitated GEF-H1 was phosphorylated with activated recombinant ERK in the presence of [^{32}P]-γ-ATP (data available upon request). ^{32}P-labelled GEF-H1 was digested with trypsin and the phosphopeptides were separated by HPLC. The radioactive peptides eluted in two peaks (data available upon request). Edman degradation of both peptide peaks indicated a phosphorylated amino acid at position 6 (data available upon request). Using MALDI-MS on the radioactive fractions, we identified the peptide in the major first peak as LSPPHpSPR (data available upon request), which corresponds to S959 in GEF-H1.

We did not identify T678, previously reported as an ERK site (16), in our *in vitro* assay. This may have been due to low phosphorylation stoichiometry of T678, as the

method used may fail to identify low abundant radiolabelled peptides. Attempts to detect changes in the phosphorylation status of this site using a generic pTP antibody were ambiguous. Therefore, we decided to quantify the phosphorylation sites by MS. Similar to western blotting, MS quantification by itself is not able to determine occupancy rates, but thanks to new analysis tools it is feasible to determine ratio changes by comparing ion intensities across samples without the need to isotopically label them. Thus, we used a label-free quantitative MS method to monitor intensity changes of GEF-H1 phosphorylation in response to MEK inhibition, both in HEK293 (data available upon request) and HCT116 cells (Figs. 2A). We readily identified multiple GEF-H1 phosphorylation sites in both cell lines. S959 phosphorylation decreased in either cell line upon treatment with U0126. Conversely, T678 phosphorylation was cell type specific. In HEK293 cells the peptide phosphorylated on T678 was readily identifiable, and represented the most intense ion of all the phosphopeptides detected. In accordance to previous reports, U0126 was able to reduce its phosphorylation. Additionally, we identified that phosphorylation of S695 was inhibited by U0126. Surprisingly, both sites were below the detection limit in HCT116 cells, despite this cell line harbouring a hyperactivated MAPK pathway. Thus, we concluded that in HCT116 cells the latter two sites appear not to be phosphorylated or are phosphorylated to a level below the detection limit, implying that the S959 is the major MEK dependent phosphorylation site in HCT116 cells. Based on these data, T678 and S695 phosphorylation is cell type dependent. It has to be noted that, despite complete inhibition of ERK phosphorylation for the duration of one hour, a substantial amount of GEF-H1 is still phosphorylated on Ser959 in HCT116 and HEK293 cells. The same holds true for Thr678 and Ser695 in HEK293 cells. This suggests that ERK is not the sole S959. T678 and S695 kinase and that

contributions from other kinases maintain GEF-H1 phosphorylation levels despite the absence of ERK activity.

Due to the absence of T678 and S695 phosphorylation, we focussed on the characterisation of S959, which is the major ERK-regulated GEF-H1 phosphorylation site in HCT116 cells. S959 has been previously shown to be a direct substrate of CDK1 and Aurora B as well as being required for PAR1b regulation of GEF-H1 activity (12, 14). First, we established that S959 is the major target phosphorylation site for ERK in GEF-H1. GEF-H1 was constitutively phosphorylated in growing conditions in HCT116 cells, (Fig. 2A). Phosphorylation was detected using an antibody that selectively recognises a phosphorylated serine on a perfect ERK consensus motif (PXpSP). This motif is unique to S959 within the GEF-H1 sequence, and the phosphorylation signal could be reduced by about 50% by the U0126 and PD0325901 MEK inhibitors (data available upon request). These results suggest that GEF-H1 is phosphorylated by ERK on S959 in a MEK dependent manner. To independently confirm the ERK-dependency of the S959 phosphorylation in another cell line, we transfected MCF7 cells with wt and S-A Flag-GEF-H1 (Fig. 2B). In the latter construct S959 was mutated to an alanine to prevent phosphorylation. The cells were serum starved and stimulated with EGF in the presence or absence of a MEK inhibitor. The phosphorylation of S959 increased within 5 minutes of EGF treatment. The augmentation was blocked by U0126 confirming the MEK dependency that we observed in HCT116 cells. No signal was detectable if S959 was mutated to alanine, confirming the specificity of the PXpSP antibody, and that S959 is phosphorylated in response to acute growth factor stimulation. Further, to demonstrate that the reduction of S959 phosphorylation was not due to an off-target effect of U0126, we repeated the experiment with an alternative MEK inhibitor, PD0325901. Conversely,

PD0325901 reduced EGF-induced S959 phosphorylation (Fig. 2C). Having established that ERK binds in an activation dependent manner and phosphorylates GEF-H1 on S959 we wanted to ascertain if GEF-H1 contains any putative ERK/MAPK binding motifs. ERKs can specifically bind to a DEF-motif and MAPKs can bind to D-domains (26). We used Scansite 2.0 (27) to predict putative interaction domains and phosphorylation sites of human GEF-H1. We detected both a DEF and D-Domain in the C-terminus of the protein. In addition, only S959 and S955 were predicted to be MAPK substrate sites (data available upon request). The DEF-domain was not conserved across mammals, whereas both the predicted phosphorylation sites and the D-domain are conserved (Fig. 2D). Thus, we found a conserved MAPK-binding and -phosphorylation site within vicinity of each other, suggesting that this is the ERK-interaction domain which targets the C-terminal phosphorylation of GEF-H1.

Phosphorylation on S959 inhibits GEF-H1 activity

GEF-H1 has been shown to be regulated by phosphorylation on multiple sites (12-14, 16, 28). Interestingly, phosphorylation on both S885 and S959 were recently reported to inhibit GEF-H1 activity (12, 14). Therefore, we examined the effects of wt GEF-H1 and the S959A (S-A) mutant on RhoA activity in growing HCT116 cells using Rhotekin pull-downs assays (Figs. 2E & F). While expression of wt GEF H1 elevated RhoA-GTP levels only marginally and insignificantly, the S-A mutation induced significant increases, confirming previous reports that S959 is an inhibitory site (12, 14). Surprisingly, the phosphomimetic S-D mutation also increased RhoA-GTP levels to a similar extent as the S-A mutation. The similar effects of the non-phosphorylatable alanine and aspartate mutations indicate that size and negative

charge of the carboxyl-group is insufficient to mimic the acidity and size of the phosphoric acid residue. In these cases substitutions by alanine are functionally equivalent to substitutions by phosphomimetic amino acids. Therefore, we conducted subsequent experiments using the S-A mutant. In order to establish if whether another phosphorylation site on GEF-H1 mediates the MEK-dependent regulation of its activity, we transfected HCT116 cells with the wt and S-A mutant and treated the cells with U0126. As expected, both the S-A mutation and U0126 treatment increased RhoA activity in comparison to wt-transfected cells, whereas MEK-inhibition had no effect on cells transfected with the S-A mutant (Fig. 2G). This result suggests that S959 is the main regulator of GEF-H1 activity downstream of the MAPK-pathway in growing HCT116 cells.

GEF-H1 has been reported to bind to microtubules when inactive. Therefore, we examined whether the inhibitory effect of S959 phosphorylation by ERK may be due to induction of microtubule binding of GEF-H1. We transfected COS-1 cells with eGFP-tagged wt and S-A mutant and treated the cells with 10 μM U0126 or DMSO. In accordance to previous reports, we detected wt GEF-H1 localised at microtubules and at the plasma membrane. Treatment with U0126 or the S-A mutation changed the localisation only marginally to a more diffuse cytoplasmatic localisation. The change in localisation was only slight (data available upon request). Therefore, we cannot conclude that the inhibitory effect of S959 phosphorylation is due to induction of microtubules binding.

S959 phosphorylation is crucial for invasiveness

Efficient cell migration depends on the close spatial and temporal coordination of RhoA, Rac and CDC42 activities. GEF-H1 can promote directional migration and

352 regulate RhoA activity at the leading edge in moving HeLa cells (11). Additionally,
353 MEK inhibition can impair cell migration, which led us to investigate whether the
354 GEF-H1 mediated cross-talk between ERK and RhoA signalling may regulate cell
355 motility. Tumour cells can move into a three dimensional environment in two basic
356 modes: they can invade in a Rac dependent mesenchymal, or a RhoA dependent
357 amoeboid fashion (7, 29). Cells can switch between these modes of invasion (29), and
358 high levels of RhoA activity can induce a more rounded amoeboid morphology. As
359 HCT116 poorly invade into Matrigel, which is used for three dimensional invasion
360 assays, we used MDA-MB-231 cells to further investigate the roles of GEF-H1 and
361 S959 phosphorylation in three-dimensional motility. MDA-MB-231 invade in a
362 mesenchymal and collective fashion. Similar to the HCT116 cell line, MDA-MB-231
363 harbour a mutant *K-RAS*^{G13D} allele, which should reduce the endogenous GEF activity
364 through stimulation of S959 phosphorylation.

365 In order to test this hypothesis, we knocked down GEF-H1 by siRNAs or inhibited the
366 ERK pathway using a chemical MEK inhibitor, and monitored RhoA activity by
367 Rhotekin pull-down experiments (Fig. 3A). Knocking down GEF-H1 approximately
368 halved the basal RhoA activity. Moreover, RhoA-GTP levels increased upon
369 administering the U0126 MEK inhibitor in a time dependent manner. Intriguingly,
370 this increase was completely blocked by GEF-H1 downregulation. Thus, at least half
371 of the RhoA activity in growing MDA-MB-231 cells is due to GEF-H1, while the
372 increase in RhoA-GTP induced by short-term MEK inhibition is completely
373 dependent on GEF-H1. In order to show that the observed increase of RhoA upon
374 MEK inhibition is not due to an off-target effect, we treated MDA-MB-231 cells with
375 an alternative MEK-inhibitor and were able to show that both U0126 and PD0325901
376 increased RhoA-GTP in MDA-MB-231 cells (Fig. 3B). Additionally, we could also

show that both inhibitors reduce GEF-H1 S959 phosphorylation and ERK binding in MDA-MB-231 cells (Fig. 3C).

To test the role GEF-H1 plays in invasion we over-expressed wt and S-A mutant GEF-H1 in MDA-MB-231 cells by transient transfection. Over-expression of wt GEF-H1 did not significantly affect three-dimensional invasion into Matrigel or RhoA activity, whereas the S-A mutant inhibited invasiveness and increased Rho-GTP levels (Fig. 3D-E, tiled images of sections available upon request). Likewise, U0126 and PD0325901also severely reduced invasion (Fig. 3F).

Interestingly, GEF-H1 S-A and MEK inhibition not only decreased the invasiveness of MDA-MB-231 cells, but also changed the morphology of the remaining invasive cells from an elongated, mesenchymal into a rounded phenotype (Fig. 3G), which is indicative of high RhoA activity. The cells expressing GEF-H1 S-A or treated with MEK inhibitor appeared rounded, very similar to A375-M2 cells, which exhibit the prototypical amoeboid mode of invasion (30), suggesting that GEF-H1 hyperactivity switches invading cells to the amoeboid morphology.

As the transition from a mesenchymal to an amoeboid phenotype could be induced by either a hyper-active GEF-H1 or MEK inhibition, we hypothesized that knocking down GEF-H1 should rescue some effects of MEK inhibition; i.e. promote invasion and/or inhibit the transition to the round phenotype. Inhibition of RhoA activation by TAT-C3 or knockdown of GEF-H1 partially salvaged cell invasion inhibited by U0126 or PD0325901 (Figs. 4A, B, tiled images of sections available upon request). Additionally, the change in morphology was indeed RhoA dependent as we could rescue the phenotype with TAT-C3 or GEF-H1 downregulation (Figs. 4C & D). We thus conclude that the shift from mesenchymal to rounded morphology upon MEK

inhibition is transmitted via GEF-H1 being dephosphorylated on S959, which leads to an increase in GEF-H1 and consequently RhoA activity, inducing the cell shape changes in a 3D matrix.

GEF-H1 is dispensable in mesenchymal but essential in amoeboid invasion

The reversal of the U0126 induced morphological transition by GEF-H1 depletion suggested that GEF-H1 may promote amoeboid invasion. Thus, we investigated how GEF-H1 knockdown by siRNA influenced mesenchymal and amoeboid invasion. Notably, the reduction of GEF-H1 had opposite effects on mesenchymal and amoeboid invasion. Reduced expression of GEF-H1 in the mesenchymally and collective invading cell-line MDA-MB-231 increased their invasive potential by ~60% (Fig. 5A, tiled images of sections available upon request). In contrast, the invasion of A375M2 cells, which predominantly invade amoeboidly, was more than halved (Fig. 5B, tiled images of sections available upon request). This observation indicates that GEF-H1 is dispensable (and maybe even inhibitory) for mesenchymal invasion, but necessary for amoeboid invasion. Therefore, we speculated that if we were able to induce a mesenchymal-amoeboid-transition (MAT) in MDA-MB-231 cells, their invasion should switch from a GEF-H1-independent to a GEF-H1-dependent mechanism. Mesenchymal invasion requires the degradation of surrounding tissue or matrix by the matrix-metallo-proteases (MMPs), and evidence suggests that MAT can be induced by inhibiting MMPs (31). Applying the broad-band MMP inhibitor GM6001, the cells became rounded and morphologically underwent MAT (Figs. 5C). When we reduced GEF-H1 levels with siRNA and monitored both MDA-MB-231 morphology and motility, GM6001 not only induced MAT, but also inhibited invasion (Fig. 5D, tiled images of sections available upon

request). GEF-H1 knockdown in combination with GM6001 did not further inhibit invasion but induced an amoeboid-mesenchymal-transition (AMT), characterised by the reappearance of elongated, mesenchymal cells in the invading fraction (Fig. 5C). In contrast to MAT induced by MEK inhibition, the knockdown and subsequent AMT did not rescue the invasiveness of the cells, probably because the presence of MMP inhibitors prevented the degradation of the Matrigel required for efficient mesenchymal invasion. The rounding of the cells is apparently independent of the ERK-pathway, as GM6001 treatment on its own only marginally reduced ERK phosphorylation in MDA-MB-231 (Fig. 5E).

Taken together these data confirm our hypothesis that GEF-H1 can drive amoeboid invasion and is pivotal for MAT induced by MMP inhibitors

Discussion

In migrating cells, leading edge RhoA activity regulates the protrusion dynamics. This highly dynamic process requires a fast response to intrinsic and extrinsic stimuli as well as coordinated cycling between active and inactive states. Previous studies have revealed a mutual antagonism between Rac and Rho signalling, whose coordination is important for the regulation of cell motility, invasiveness and mode of invasiveness (for a recent review see (31)). High Rac activity promotes the mesenchymal mode of invasion, while high Rho activity facilitates amoeboid movement. The chain of events regulating Rac activation in migration was recently elucidated as a cascade of the adaptor protein NEDD9 recruiting the Rac-specific GEF DOCK3, which activates Rac1 (5). However, the GEF, which activates Rho, is unknown. Our data suggest that this GEF is GEF-H1.

The known properties of GEF-H1 are consistent with a pivotal role upstream of RhoA in regulating RhoA mediated protrusion dynamics. GEF-H1 activity is tightly regulated by microtubule binding, and microtubule disassembly by nocodazole induces a robust and fast activation of RhoA via GEF-H1 (19, 28). In addition to microtubule binding GEF-H1 activity is suppressed intrinsically by its C-terminal domain. Cleavage of this regulatory domain is sufficient to transform GEF-H1 into a potent oncogene (32). The C-terminal regulatory domain contains a multitude of phosphorylation sites and functions as a hub for integrating upstream signalling. Aside from PAK (13, 28) AuroraA, Cdk1/CyclinB, and Par1b (12) phosphorylate GEF-H1 on inhibitory sites in the C-terminus. Here, we here have identified ERK as a kinase that can inhibit GEF-H1 activity by phosphorylating S959 in this C-terminal region in response to acute growth factor stimulation or under growing conditions. Our results contrast with previous reports which have shown a MEK-dependent activation of GEF-H1 via a direct ERK phosphorylation. Although at first sight our results are diametrically opposite, ERK-dependent activation of RhoA and GEF-H1 has been observed downstream of stress signalling, such as TNFα and membrane de-polarisation. It is plausible that upon activation of stress signals several pathways are activated which result in the formation of an ERK/Scaffold/GEF-H1 complex which enables ERK to phosphorylate Thr678 efficiently. Additionally, we have observed that in embryo-derived HEK293 cells T678, S695 and S959 phosphorylations are reduced upon MEK inhibition, whereas, in the colon cancer cell line HCT116, only S959 phophorylation is detectable and responds to U0126 treatment. These data suggests that the pattern of GEF-H1 phosphorylation is cell type dependent.

MEK inhibition or the GEF-H1 S959A mutation has dramatic effects on cells embedded in a three dimensional matrix. MDA-MB-231 cells invade into collagen or

Matrigel as elongated cells in a mesenchymal fashion. Inhibition of the ERK pathway almost completely prevents the cells from invading towards an EGF or serum gradient, and more interestingly, also causes the cells to change their morphology. They become rounded and resemble cells which invade in an amoeboid fashion. This change in shape is also enforced by expressing a GEF-H1 mutant that cannot be phosphorylated on S959. This change in morphology, and to a lesser extent the deficient motility, can be rescued by either suppressing RhoA signalling or by reducing endogenous levels of GEF-H1. Taken together, these data reveal a mechanism how ERK can regulate cell motility and invasiveness by crosstalking to the RhoA pathway (Fig. 6). They also suggest that the transition of a mesenchymal to amoeboid morphology can be induced by GEF-H1, and that amoeboid invasion in A375M2 cells is dependent on GEF-H1.

GEF-H1 is frequently expressed to high levels in cancers (www.proteinatlas.org), and we were surprised to find that GEF-H1 expression was subduing the invasive potential of MDA-MB-231 cells. A plausible explanation is that the ability of cancer cells to switch between mesenchymal and amoeboid modes of movement may be advantageous to invade surrounding tissue. GEF-H1 can be easily inactivated by high ERK activity when mesenchymal invasion is preferred. On the other hand, high levels of GEF-H1 activity will facilitate transition to an amoeboid type of invasion. This plasticity would enable a cell to maintain high invasive motility regardless of its environment.

Acknowledgements

We thank Gary Bokoch and Mike Olson for sharing their plasmids and reagents with us, David Matallanas and Dan Croft for helping us with the RhoA-GTP pull-downs, Natalia Volinsky and Drieke Vandamme for comments, Cancer Research UK, the European Union FP6 interaction proteome and Science Foundation Ireland (Grant 06/CE/B1129) for financial support.

References

1. **Machacek M, Hodgson L, Welch C, Elliott H, Pertz O, Nalbant P, Abell A, Johnson GL, Hahn KM, Danuser G.** 2009. Coordination of Rho GTPase activities during cell protrusion. Nature **461:**99-103.

2. **Kurokawa K, Matsuda M.** 2005. Localized RhoA activation as a requirement for the induction of membrane ruffling. Mol Biol Cell **16:**4294-4303.

3. **Pertz O, Hodgson L, Klemke RL, Hahn KM.** 2006. Spatiotemporal dynamics of RhoA activity in migrating cells. Nature **440:**1069-1072.

4. **McGhee EJ, Morton JP, Von Kriegsheim A, Schwarz JP, Karim SA, Carragher NO, Sansom OJ, Anderson KI, Timpson P.** 2011. FLIM-FRET imaging in vivo reveals 3D-environment spatially regulates RhoGTPase activity during cancer cell invasion. Small GTPases **2:**239-244.

5. **Sanz-Moreno V, Gadea G, Ahn J, Paterson H, Marra P, Pinner S, Sahai E, Marshall CJ.** 2008. Rac activation and inactivation control plasticity of tumor cell movement. Cell **135:**510-523.

6. **Rottner K, Hall A, Small JV.** 1999. Interplay between Rac and Rho in the control of substrate contact dynamics. Curr Biol **9:**640-648.

7. **Sahai E, Marshall CJ.** 2003. Differing modes of tumour cell invasion have distinct requirements for Rho/ROCK signalling and extracellular proteolysis. Nat Cell Biol **5:**711-719.

8. **Pankova K, Rosel D, Novotny M, Brabek J.** 2010. The molecular mechanisms of transition between mesenchymal and amoeboid invasiveness in tumor cells. Cell Mol Life Sci **67:**63-71.

9. **Wolf K, Wu YI, Liu Y, Geiger J, Tam E, Overall C, Stack MS, Friedl P.** 2007. Multi-step pericellular proteolysis controls the transition from individual to collective cancer cell invasion. Nat Cell Biol **9:**893-904.

10. **Rossman KL, Der CJ, Sondek J.** 2005. GEF means go: turning on RHO GTPases with guanine nucleotide-exchange factors. Nat Rev Mol Cell Biol **6:**167-180.

11. **Nalbant P, Chang YC, Birkenfeld J, Chang ZF, Bokoch GM.** 2009. Guanine nucleotide exchange factor-H1 regulates cell migration via localized activation of RhoA at the leading edge. Mol Biol Cell **20:**4070-4082.

12. **Birkenfeld J, Nalbant P, Bohl BP, Pertz O, Hahn KM, Bokoch GM.** 2007. GEF-H1 modulates localized RhoA activation during cytokinesis under the control of mitotic kinases. Dev Cell **12:**699-712.

13. **Callow MG, Zozulya S, Gishizky ML, Jallal B, Smeal T.** 2005. PAK4 mediates morphological changes through the regulation of GEF-H1. Journal of cell science **118:**1861-1872.

14. **Yamahashi Y, Saito Y, Murata-Kamiya N, Hatakeyama M.** 2011. Polarity-regulating kinase partitioning-defective 1b (PAR1b) phosphorylates guanine nucleotide exchange factor H1 (GEF-H1) to regulate RhoA-dependent actin cytoskeletal reorganization. The Journal of biological chemistry **286:**44576-44584.

15. **Yoshimura Y, Miki H.** 2011. Dynamic regulation of GEF-H1 localization at microtubules by Par1b/MARK2. Biochemical and biophysical research communications **408:**322-328.

16. **Fujishiro SH, Tanimura S, Mure S, Kashimoto Y, Watanabe K, Kohno M.** 2008. ERK1/2 phosphorylate GEF-H1 to enhance its guanine nucleotide exchange activity toward RhoA. Biochemical and biophysical research communications **368:**162-167.

17. **Guilluy C, Swaminathan V, Garcia-Mata R, O'Brien ET, Superfine R, Burridge K.** 2011. The Rho GEFs LARG and GEF-H1 regulate the mechanical response to force on integrins. Nat Cell Biol **13:**722-727.

18. **Kakiashvili E, Speight P, Waheed F, Seth R, Lodyga M, Tanimura S, Kohno M, Rotstein OD, Kapus A, Szaszi K.** 2009. GEF-H1 mediates tumor necrosis factor-alpha-induced Rho activation and myosin phosphorylation: role in the regulation of tubular paracellular permeability. J Biol Chem **284:**11454-11466.

19. **Chang YC, Nalbant P, Birkenfeld J, Chang ZF, Bokoch GM.** 2008. GEF-H1 couples nocodazole-induced microtubule disassembly to cell contractility via RhoA. Mol Biol Cell **19:**2147-2153.

20. **Hennigan RF, Hawker KL, Ozanne BW.** 1994. Fos-transformation activates genes associated with invasion. Oncogene **9:**3591-3600.

21. **von Thun A, Birtwistle M, Kalna G, Grindlay J, Strachan D, Kolch W, von Kriegsheim A, Norman JC.** 2012. ERK2 drives tumour cell migration in three-dimensional microenvironments by suppressing expression of Rab17 and liprin-beta2. Journal of cell science **125:**1465-1477.

22. **von Kriegsheim A, Baiocchi D, Birtwistle M, Sumpton D, Bienvenut W, Morrice N, Yamada K, Lamond A, Kalna G, Orton R, Gilbert D, Kolch W.** 2009. Cell fate decisions are specified by the dynamic ERK interactome. Nat Cell Biol **11:**1458-1464.

23. **Rappsilber J, Ishihama Y, Mann M.** 2003. Stop and go extraction tips for matrix-assisted laser desorption/ionization, nanoelectrospray, and LC/MS sample pretreatment in proteomics. Anal Chem **75:**663-670.

24. **Pollock CB, Shirasawa S, Sasazuki T, Kolch W, Dhillon AS.** 2005. Oncogenic K-RAS is required to maintain changes in cytoskeletal organization, adhesion, and motility in colon cancer cells. Cancer Res **65:**1244-1250.

25. **Vial E, Sahai E, Marshall CJ.** 2003. ERK-MAPK signaling coordinately regulates activity of Rac1 and RhoA for tumor cell motility. Cancer Cell **4:**67-79.

584 26. **Tanoue T, Nishida E.** 2003. Molecular recognitions in the MAP kinase
585 cascades. Cell Signal **15:**455-462.

586 27. **Obenauer JC, Cantley LC, Yaffe MB.** 2003. Scansite 2.0: Proteome-wide
587 prediction of cell signaling interactions using short sequence motifs. Nucleic
588 Acids Res **31:**3635-3641.

589 28. **Zenke FT, Krendel M, DerMardirossian C, King CC, Bohl BP, Bokoch**
590 **GM.** 2004. p21-activated kinase 1 phosphorylates and regulates 14-3-3
591 binding to GEF-H1, a microtubule-localized Rho exchange factor. J Biol
592 Chem **279:**18392-18400.

593 29. **Friedl P.** 2004. Prespecification and plasticity: shifting mechanisms of cell
594 migration. Curr Opin Cell Biol **16:**14-23.

595 30. **Wilkinson S, Paterson HF, Marshall CJ.** 2005. Cdc42-MRCK and Rho-
596 ROCK signalling cooperate in myosin phosphorylation and cell invasion. Nat
597 Cell Biol **7:**255-261.

598 31. **Symons M, Segall JE.** 2009. Rac and Rho driving tumor invasion: who's at
599 the wheel? Genome Biol **10:**213.

600 32. **Whitehead I, Kirk H, Tognon C, Trigo-Gonzalez G, Kay R.** 1995.
601 Expression cloning of lfc, a novel oncogene with structural similarities to
602 guanine nucleotide exchange factors and to the regulatory region of protein
603 kinase C. J Biol Chem **270:**18388-18395.
604
605
606

Figure Legends

Fig. 1. MEK inhibition elevates RhoA-GTP levels and reduces ERK association with GEF-H1

(A) RhoA-GTP was precipitated with Rhothekin-GST beads from HCT116 cells treated with 10 μM U0126 for the indicated times. Values are means ± standard deviation (s.d.). **(B)** Representative Western blot of RhoA-GTP pulled down with Rhothekin-GST beads. Cell lysates and Rhothekin-pulldown were blotted with indicated antibodies. **(C)** Western blot analysis of the effects of long-term MEK inhibition on pERK and Fra-1 expression in HCT116 cells. **(D)** Growing HCT116 cells growing in 10% FCS were incubated with DMSO or U0126 10 μM for 1h. Endogenous ERK1 and ERK2 was immunoprecipitated and Western blotted with the indicated antibodies. A mock immunoprecipitation with protein Protein-A beads was used as control.

Fig. 2. ERK phosphorylation of S959 inhibits GEF-H1 activity

(A) GEF-H1 phospho-peptides and corresponding peptides were identified by MS/MS from HCT116 cells transfected with eGFP-GEF-H1. 48 hours post-transfection the cells treated with 10 μM U0126 for 1 hour and GEF-H1 was enriched with anti-EGFP agarose. Bar graphs represent the normalised intensities of phosphorylated peptides derived from the ion-intensities determined by the MaxQuant software. The bar graphs represent mean of three independent experiments ± s.e.m. * $p<0.05$ **(B)** MCF7 cells were transfected with Flag-GEF-H1 WT and mutant Flag-GEF-H1 S959A (S-A), serum starved (Strvd) overnight and pretreated with 10 μM U0126 or DMSO for 30 minutes and stimulated with 20 ng/ml EGF for 5 minutes. Immunoprecipitated

Flag-GEF-H1 was Western blotted with antibodies against Flag and the ERK consensus phosphorylation site PXpSP. **(C)** MCF7 cells were transfected with Flag-GEF-H1 WT, serum starved (Strvd) overnight and pretreated with 10 μM U0126, 2 μM PD0325901 or DMSO for 30 minutes and stimulated with 20 ng/ml EGF for 5 minutes and western blotted as in (C) **(D)** Mammalian GEF-H1 isoforms were aligned by Clustal-Ω. Amino acids which form the D-Domain (red) and the ERK phosphorylation motif (blue) are conserved across the species **(E)** HCT116 cells were transfected with empty vector (EV), Flag-GEF-H1 wt and S959A (S-A) mutant. RhoA-GTP was precipitated with Rhothekin-GST beads 48 hours post transfection. The bar graph represents the average of RhoA-GTP levels observed in three independent experiments. Error bars represent s.d. **(F)** Representative Western blots of RhoA-GTP precipitated with Rhothekin-GST beads and of total lysates from one of the experiments in panel D. **(G)** HCT116 cells were transfected with Flag-GEF-H1 wt and S959A (S-A) mutant and incubated with DMSO, 10 μM U0126 for 1 hour 48 hours post-transfection. RhoA-GTP was precipitated with Rhothekin-GST beads. Cell lysates and Rhothekin-pulldown were blotted with indicated antibodies. Intensities were quantified by densitometry.

Fig. 3. ERK signalling regulates motility and cell morphology via GEF-H1

(A) GEF-H1 was knocked down by siRNA in MDA-MB-231 cells. 48 hours later cells were treated with 10 μM of the MEK inhibitor U0126 for the indicated times. RhoA-GTP was precipitated with Rhothekin-GST beads. The bar graphs represent means of three independent experiments ± s.d. Western blots show a representative example. **(B)** RhoA-GTP was precipitated with Rhothekin-GST beads from MDA-MB-231 cells treated with DMSO, 10 μM U0126 or 2 μM PD0325901 for one hour.

Cell lysates and Rhothekin-pulldown were blotted with indicated antibodies. Intensities were quantified by densitometry **(C)** MDA-MB-231 cells were transfected with Flag-GEF-H1 and 24 hours post-transfection incubated with 10 μM U0126, 2 μM PD0325901 or DMSO in 10% Serum for one hour. Immunoprecipitated Flag-GEF-H1 and lysates were Western blotted with antibodies as indicated. **(D)** MDA-MB-231 cells were transfected with wt GEF-H1, S-A mutant or empty vector (EV) and subjected to an invasion assay 48 hours post-transfection. The expression of the GEF-H1 constructs was monitored by Western blotting. Invasion was quantified by measuring the fluorescence intensity of cells penetrating the Matrigel ≥45 μm. * $p<0.05$ **(E)** MDA-MB-231 cells were transfected with eGFP, eGFP-GEF-H1 wt and S959A (S-A) mutant. RhoA-GTP was precipitated with Rhothekin-GST beads 48 hours post transfection. Lysate and Rhotekin-pulldown were blotted with indicated antibodies. Intensities were quantified by densitometry **(F)** Graph representing invasion, normalized to the control, of MDA-MB-231 cells incubated with DMSO, 10 μM U0126 or 2 μM PD0325901. Invasion was quantified by measuring the fluorescence intensity of cells penetrating the Matrigel ≥45 μm. * $p<0.05$ **(G)** Cells transfected and treated as indicated were stained with calcein-AM and photographed using confocal microscopy at the 30 μm penetration plane into Matrigel. Morphological changes were quantified using ImageJ. Error bars in all panels represent standard error of the mean (s.e.m). * $p<0.05$

Fig. 4. The effects of MEK inhibition on invasion and morphology are specifically mediated by GEF-H1

(A) Graph representing invasion of MDA-MB-231 cells untreated or treated with 10 μM U0126, 2 μM PD0325901 or with the Rho inhibitor TAT-C3, and transfected

with non-targeting siRNA (NT) or oligos against GEF-H1. Invasion was quantified by measuring the fluorescence intensity of cells penetrating the Matrigel ≥45 μm. * $p<0.05$ **(B)** Western blot showing GEF-H1 knockdown efficiency after 48 hours. **(C)** Cells transfected and treated as indicated were stained with calcein-AM and imaged by confocal microscopy at the 0 and 30μm penetration planes into Matrigel. In all panels error bars represent s.e.m. **(D)** Quantitation of elongated and rounded cells of (C) * $p<0.05$.

Fig. 5. GEF-H1 is necessary for amoeboid transition and invasion

(A) Graph representing mesenchymal invasion of MDA-MB-231 cells transfected with siRNA SMARTpools (SP) or single oligos (#) against GEF-H1 as indicated. Non-targeting siRNA (NT) was used as control. Invasion was quantified by measuring the fluorescence intensity of cells penetrating the Matrigel ≥45 μm. * $p<0.05$ **(B)** Graph representing amoeboid invasion of A375M2 cells transfected with siRNA SMARTpools against GEF-H1 as indicated. Invasion was quantified as in A. * $p<0.05$ **(C)** Cells transfected and treated as indicated were stained with calcein-AM and imaged by confocal microscopy at the 30 μm penetration plane into Matrigel. Morphological changes were quantified in ImageJ. * $p<0.05$ (**D)** Graph representing invasion of MDA-MB-231 cells treated with the MMP inhibitor GM6001 and transfected with siRNA SMARTpools against GEF-H1 as indicated. Invasion was quantified as in A. * $p<0.05$ **(E)** MDA-MB-231 were seeded onto a thick layer of polymerised 4% collagen and treated with DMSO, 10 μM U0126 or 10 μM GM6001 for 24 hours. Cells were lysed and collagen was separated by centrifugation. Cleared lysates were Western blotted with indicated antibodies

Fig. 6. Summary of experimental findings

In K-Ras V12 mutant cell lines high levels of active ERK inhibit GEF-H1 by phosphorylating the exchange factor at S959. This leads to a decrease in RhoA-GTP levels, which promotes mesenchymal invasion in vitro. In contrast, inhibition of ERK signaling with U0126 stimulates RhoA activity and promotes amoeboid invasion.

von Thun Fig. 1

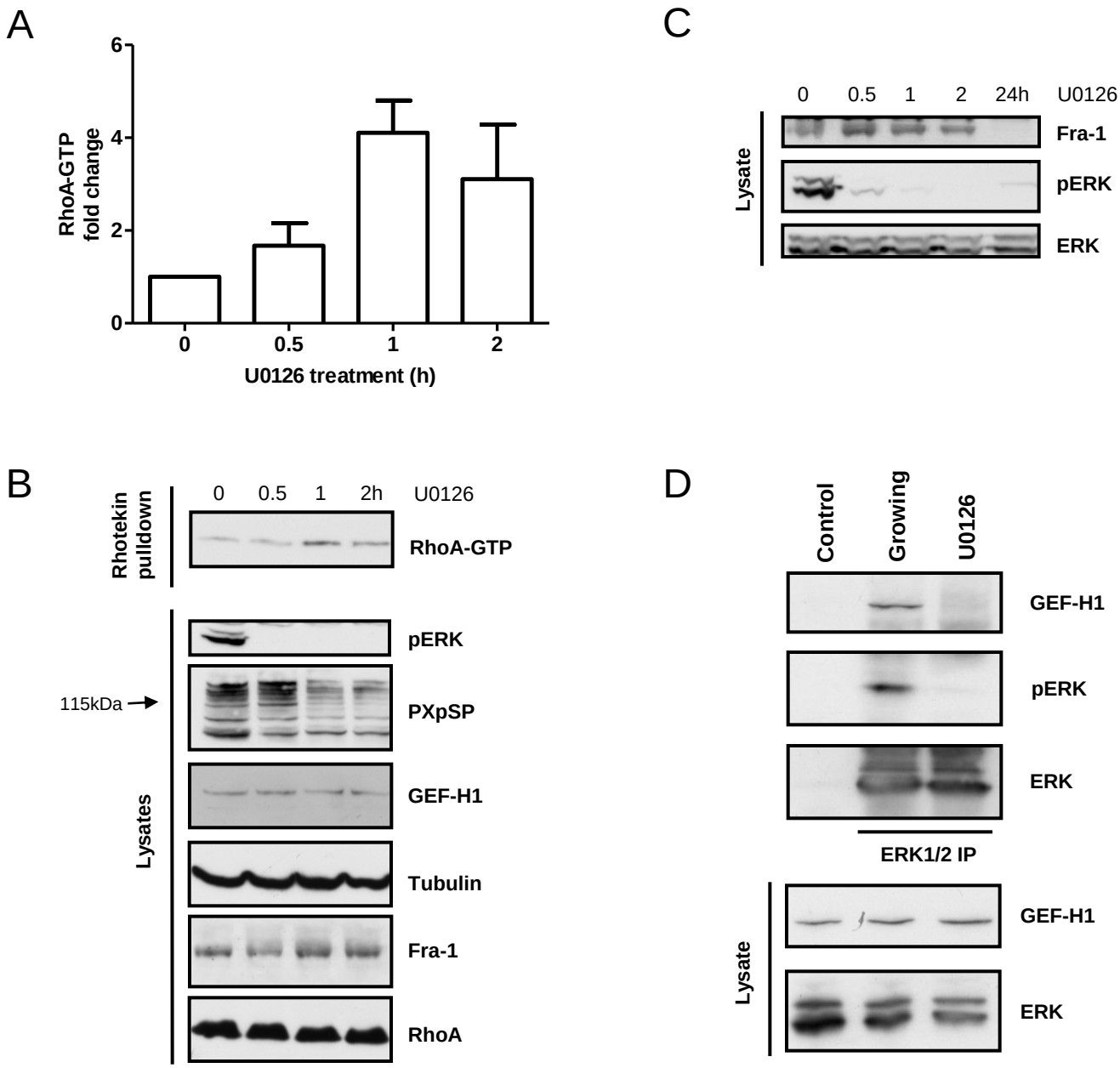

von Thun Fig. 2

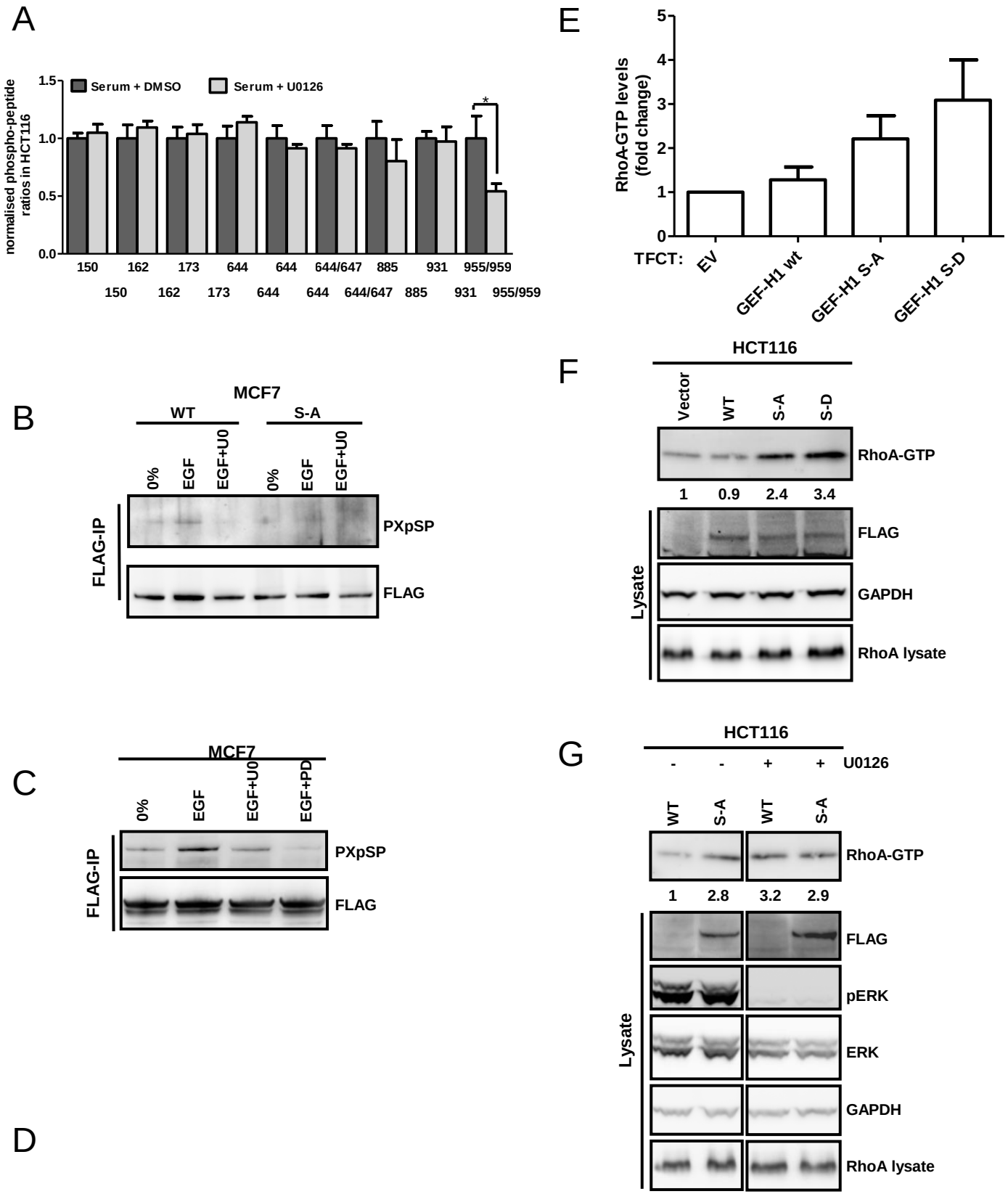

von Thun Fig. 3

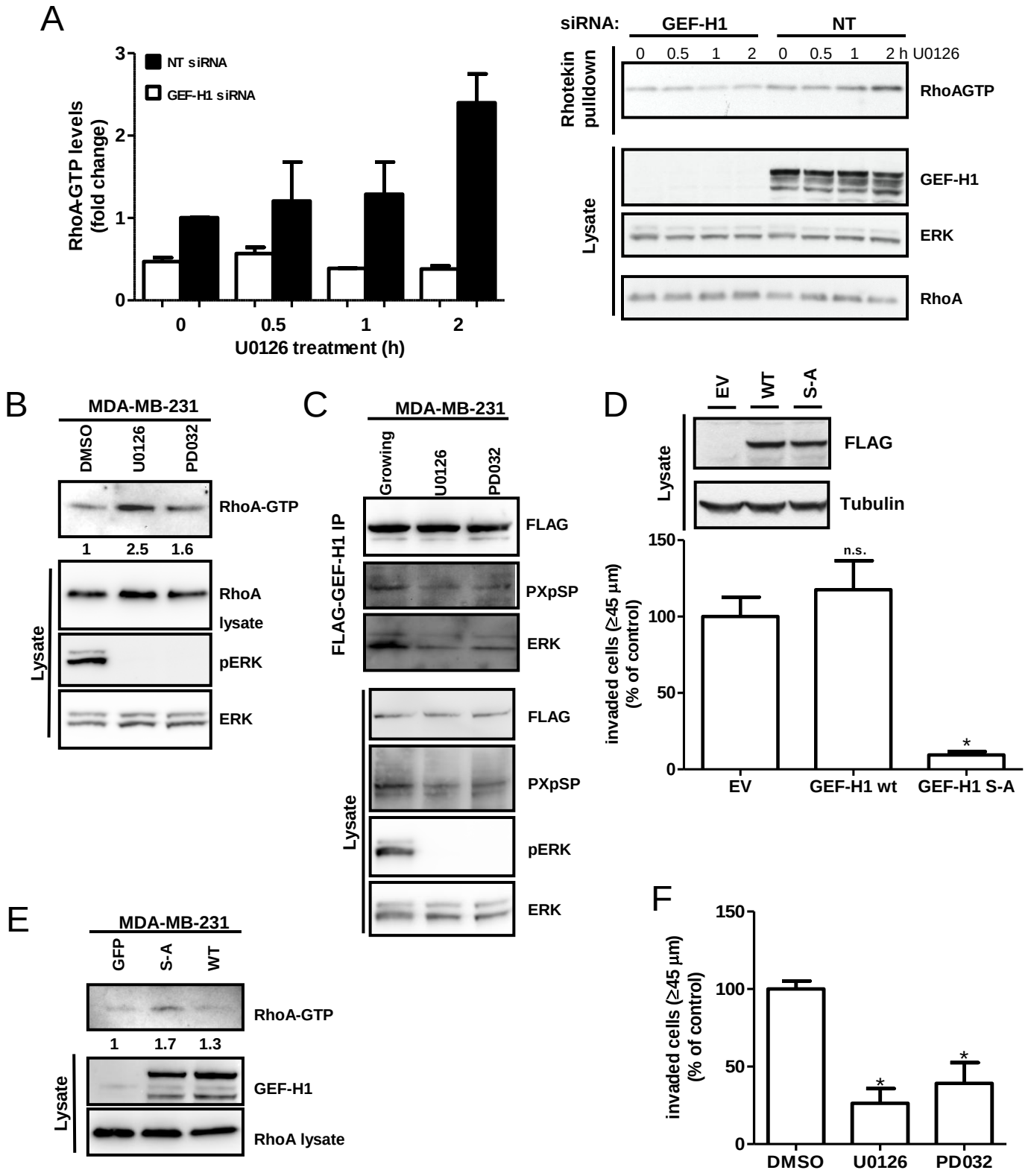

von Thun Fig. 3

G

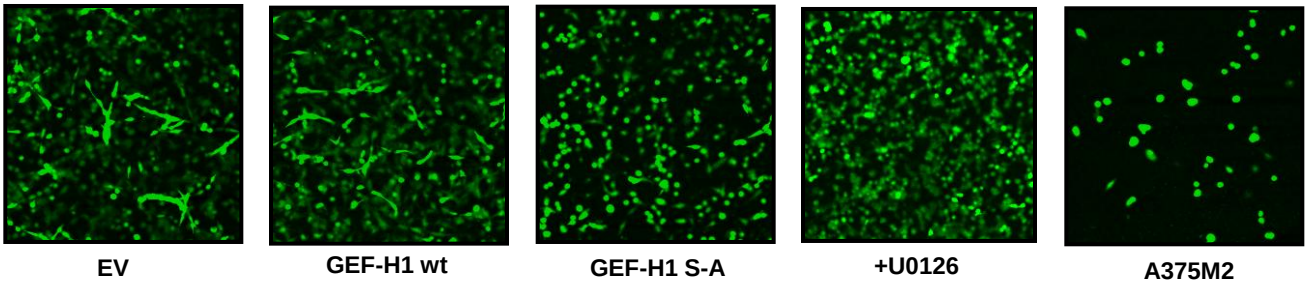

G

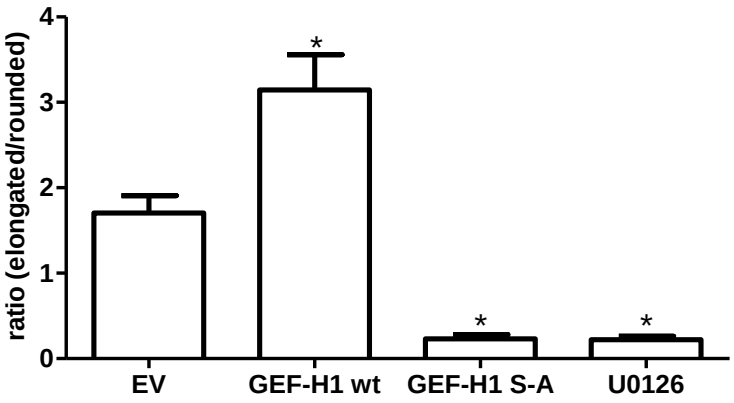

von Thun Fig. 4

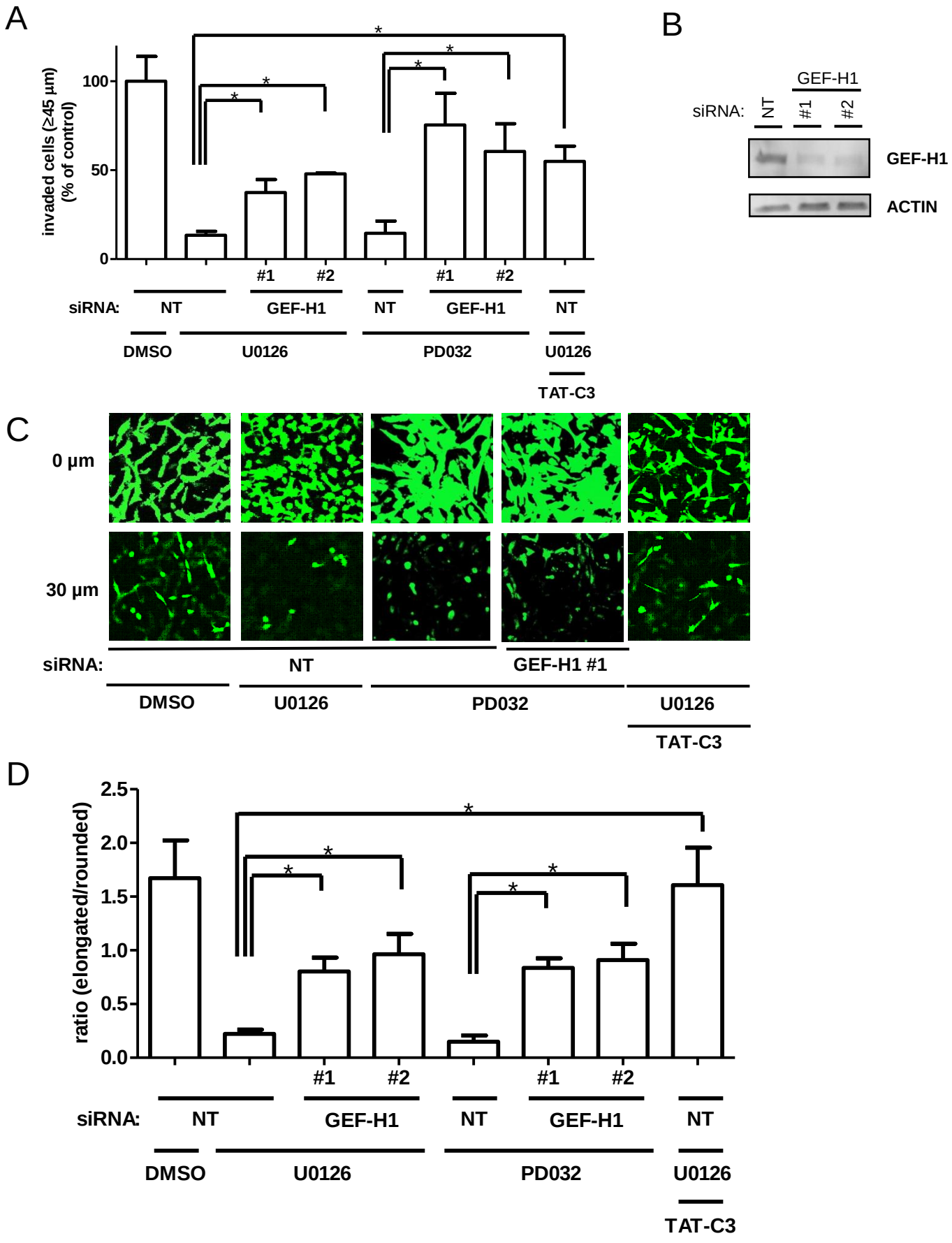

von Thun Fig. 5

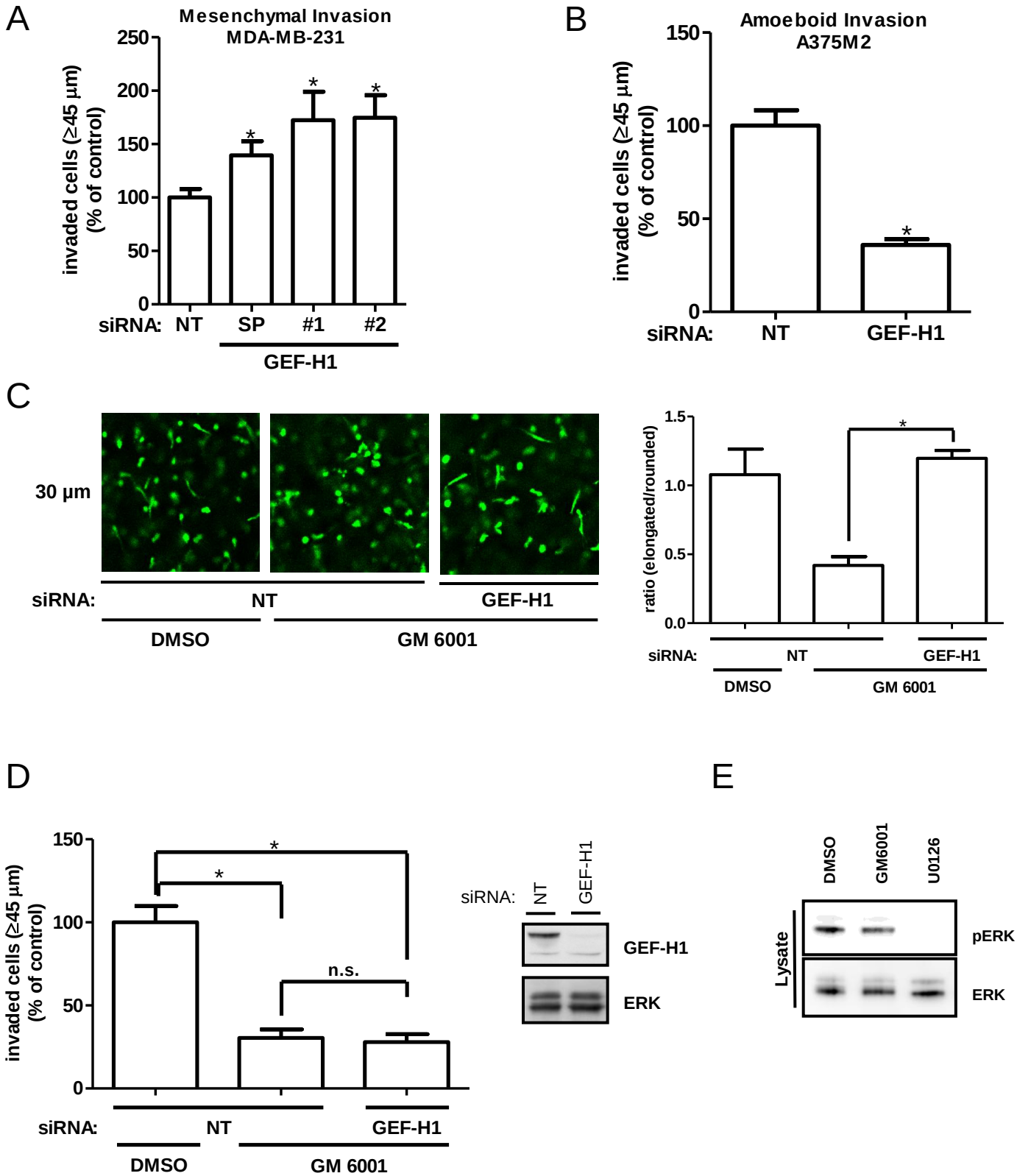

von Thun Fig. 6

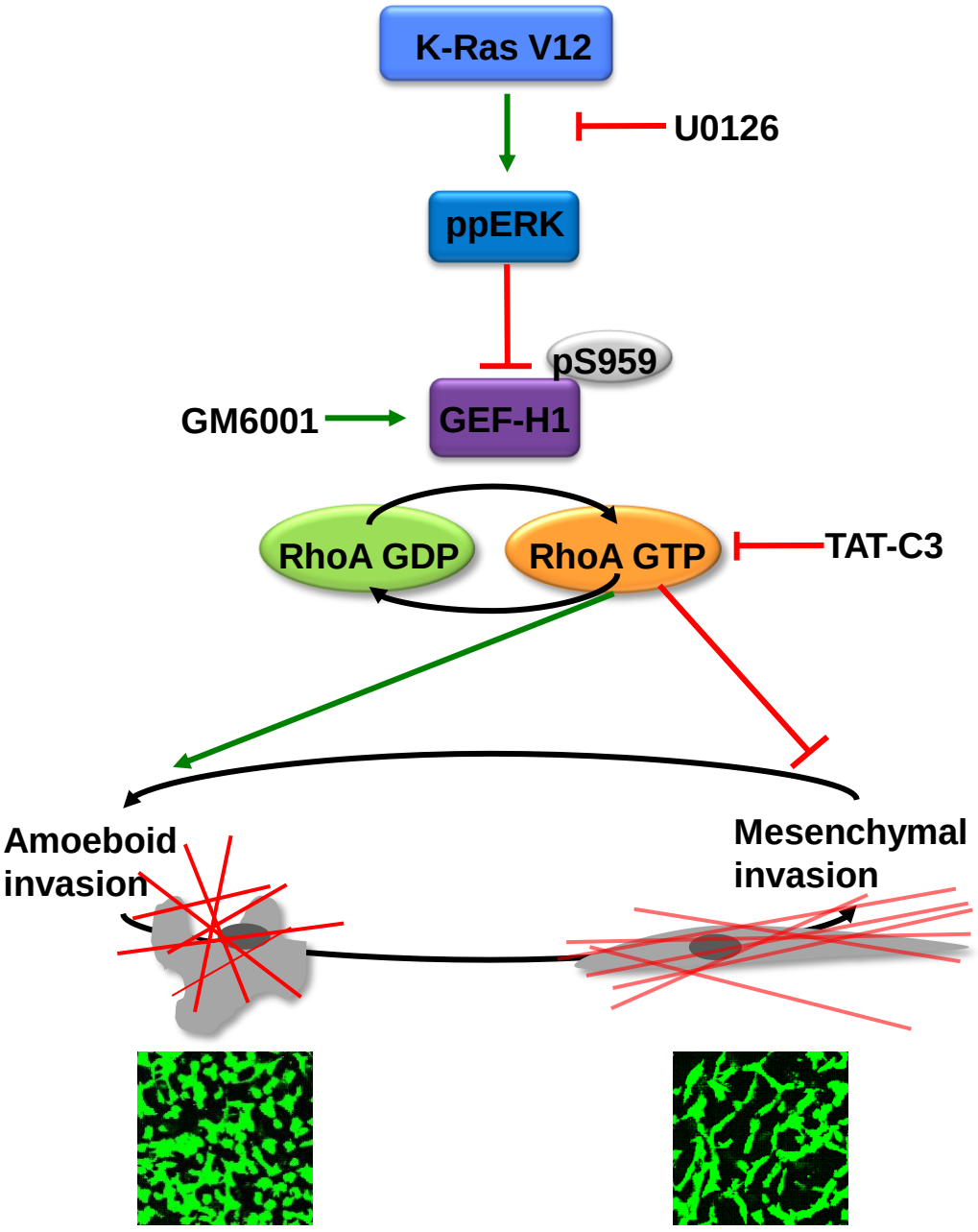

Supplemental Figure Legends

Fig. S1. ERK interacts with GEF-H1 in an activation dependent manner

(A) Serum starved (Strvd) PC12 cells were stimulated with 20 ng/ml EGF as indicated. Endogenous ERK1 was immunoprecipitated and Western blotted with the indicated antibodies. **(B)** PC12 cells were transfected a with Flag-GEF-H1 expressing plasmid. The cells were serum starved (Strvd) and stimulated with 20 ng/ml EGF for the indicated time-points. GEF-H1 was immunoprecipitated and Western blotted with the indicated antibodies. **(C)** HCT116 cells were transfected with a Flag-GEF-H1 expressing plasmid or an empty control plasmid (EV). 48 hours post-transfection were treated with 10 μM U0126 for one hour. Flag-immunoprecipitates and total lysates were western blotted with the indicated antibodies.

Fig. S2. ERK phosphorylates GEF-H1 on serine 959

(A) GEF-H1 was overexpressed in HEK293 cells. Immunoprecipitated GEF-H1 and myelin basic protein (MBP), a known ERK substrate used as control, were incubated with active ERK and [32P]-γ-ATP. The kinase assays were separated by SDS-PAGE. One gel was stained with Coomassie Blue, the second was blotted onto a PVDF membrane, and the radioactive bands were imaged with a phosphoimager. **(B)** The Coomassie band representing [32P]-labelled GEF-H1 in panel A was excised, in-gel digested with trypsin and separated by reverse-phase C18-HPLC. The image represents [32P] intensities eluting. **(C)** Edman degradation of fractions I and II from B. In both fractions amino acid 6 is labelled with [32P]. **(D)** MALDI mass spectrum of fraction I, identifying the tryptic peptide LSPPHpSPR. **(E)** Ion intensities of GEF-

H1 phosphorylation sites identified in eGFP-GEF-H1 expressed in HEK293 cells. Cells grown in DMEM with 10% serum were either treated with 10 μM U0126 or DMSO for 30 minutes. The bar graphs represent mean of three independent experiments ± s.e.m. **(F)** Ion intensities of GEF-H1 phosphorylation sites identified in eGFP-GEF-H1 expressed in HCT116 cells. Cells grown in DMEM with 10% serum were either treated with 10 μM U0126 or DMSO for 30 minutes. The bar graphs represent mean of three independent experiments ± s.e.m. **(G)** HCT116 cells were transfected with Flag-GEF-H1 and incubated with DMSO, 10 μM U0126 or 2 μM PD0325901 for 1 hour 48 hours post-transfection. Immunoprecipitated Flag-GEF-H1 was Western blotted with antibodies against Flag and the ERK consensus phosphorylation site PXpSP.

Fig. S3. Representative strips of invasion assays

Post-invasion cells were stained with Calecin-AM. 15 μM sections were scanned individually on a laser-scanning microscope and combined into a single strip. Representative tracks of the indicated Figures are shown.

Fig. S4. Subcellular localisation of GEF-H1

COS-1 cells were transfected with EGFP-GEF-H1 wt and the S959A mutant and seeded on glass cover slips. 24 hours post-transfection the cells were treated with DMSO or 10 μM U0126 for 1 hour. The cells were fixed with para-formaldehyde and mounted onto glass slides and imaged with a laser scanning confocal microscope.

Fig. S5. Scansite predictions of ERK binding and phosphorylation sites

Predicted ERK1 substrate sites, ERK-binding (DEF-domain and D domains) in human GEF-H1 (ARHG2_HUMAN). Significance threshold was selected to "medium"

von Thun Fig. S1

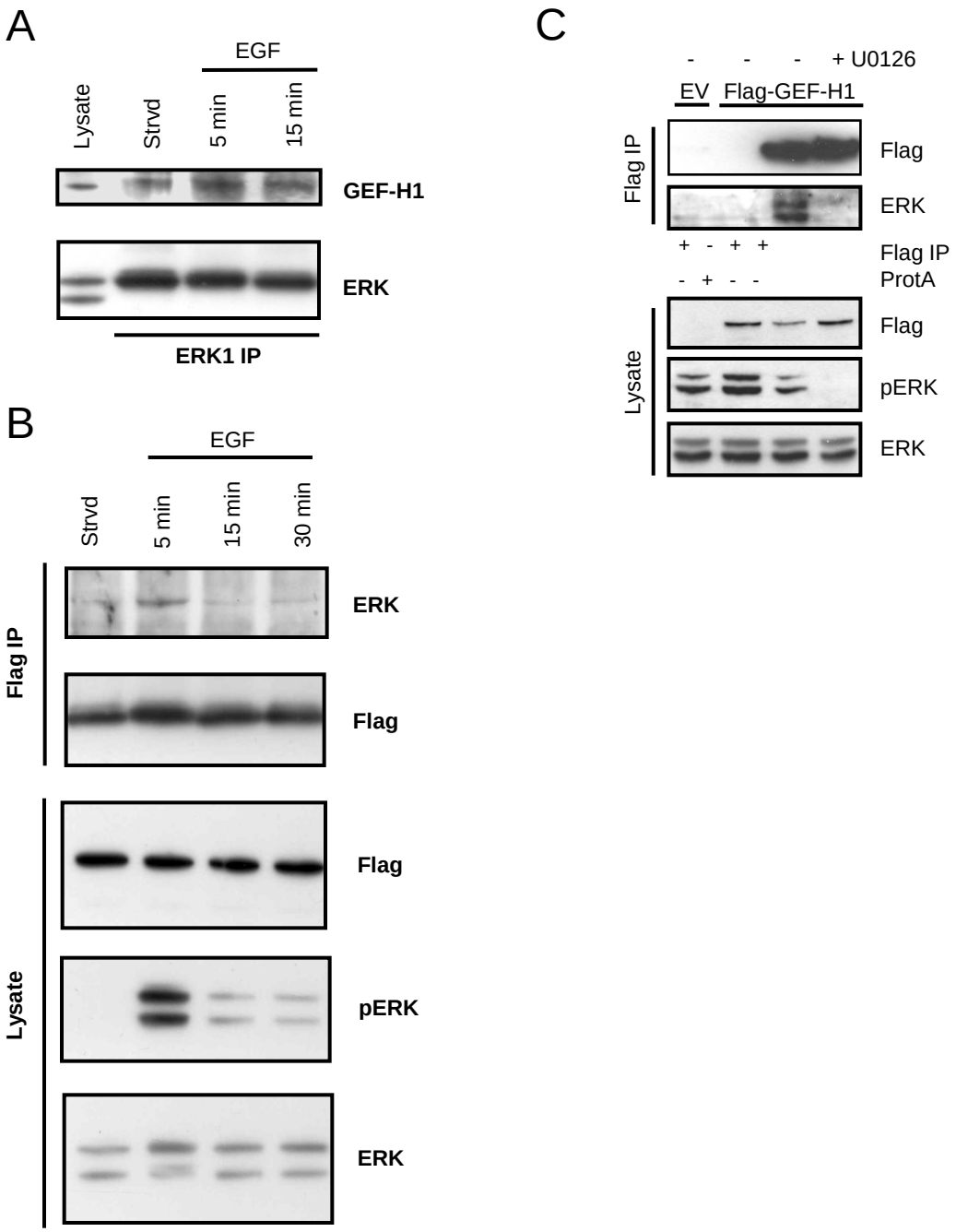

von Thun Fig. S2

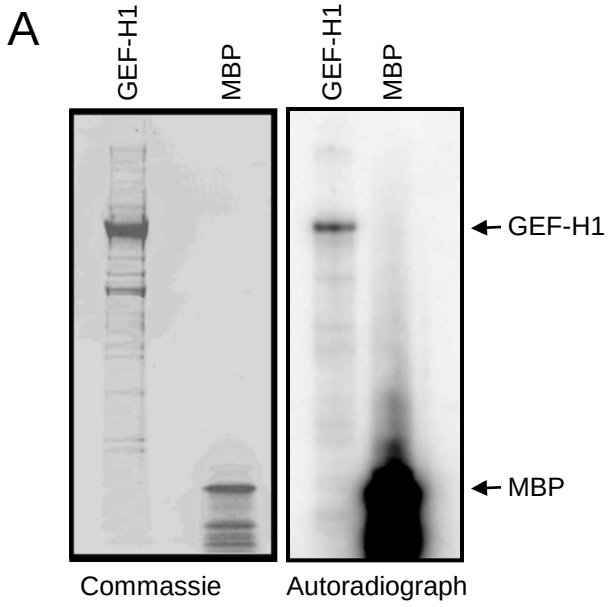

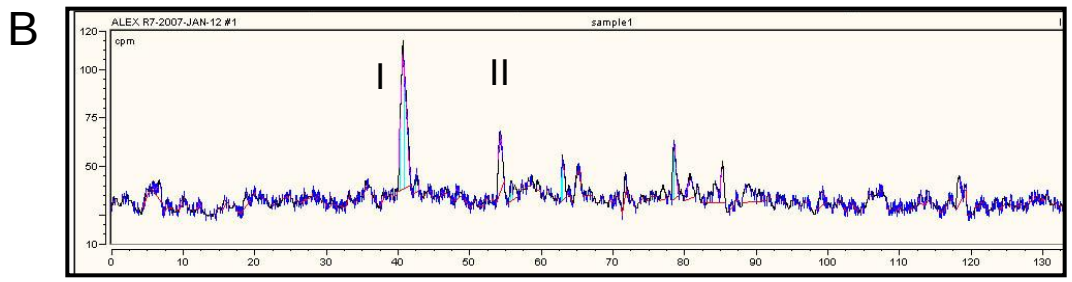

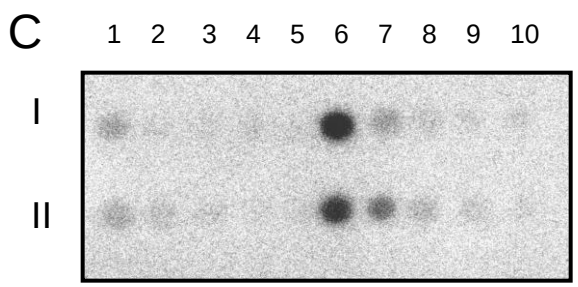

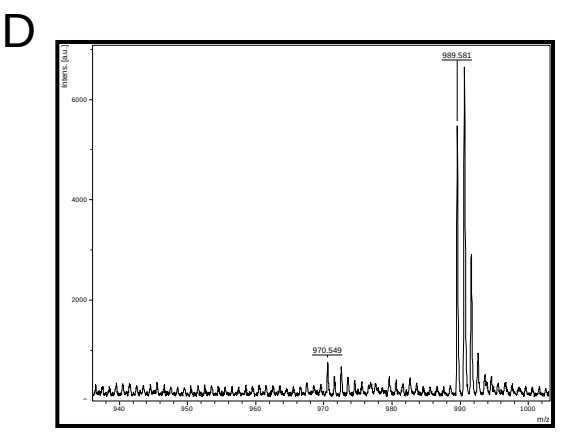

LSPPHSPR +PO_4

von Thun Fig. S2

E

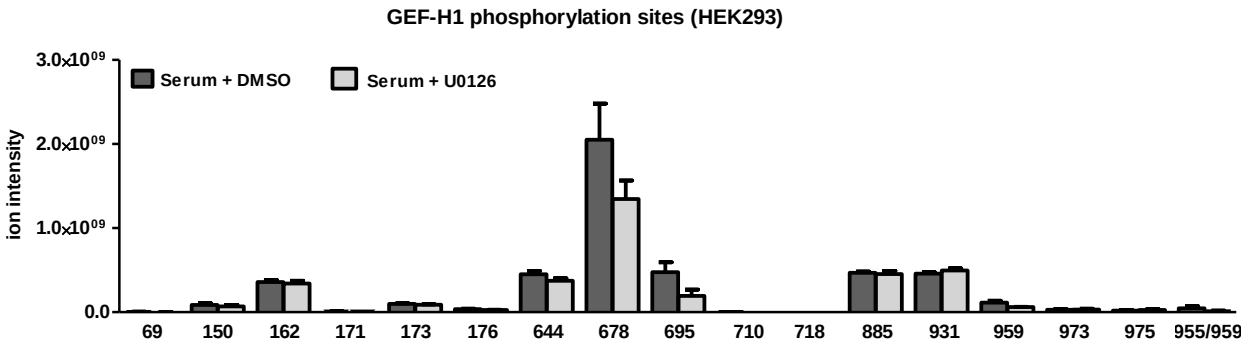

F

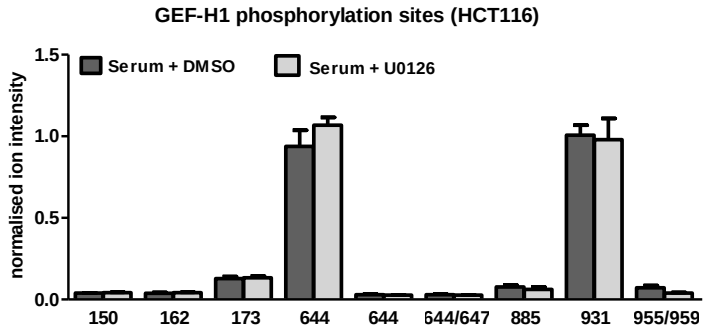

G

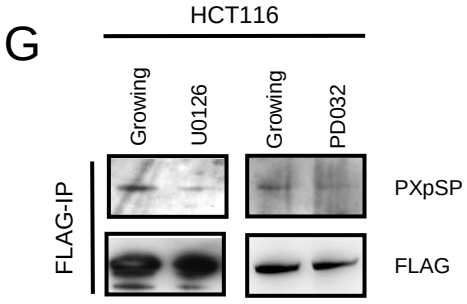

von Thun Fig. S3

Figure 3D

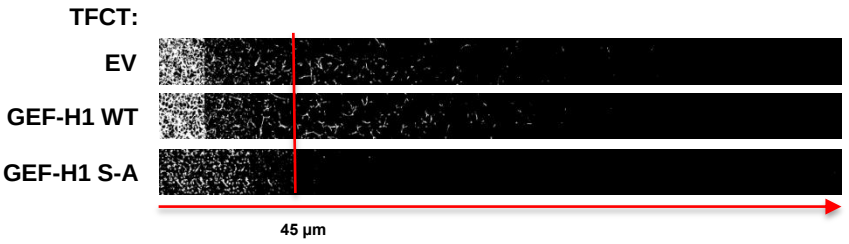

Figure 4A

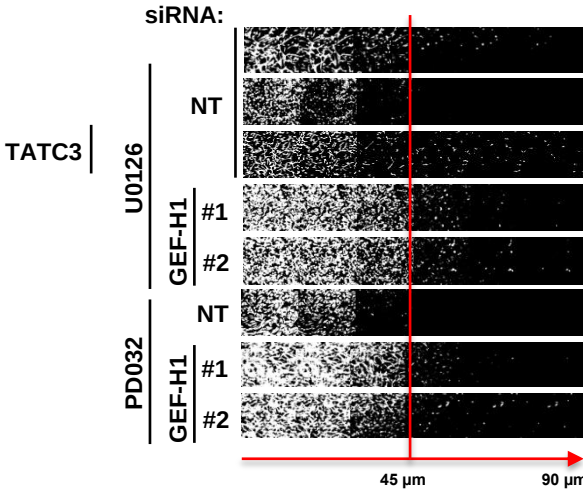

Figure 5A

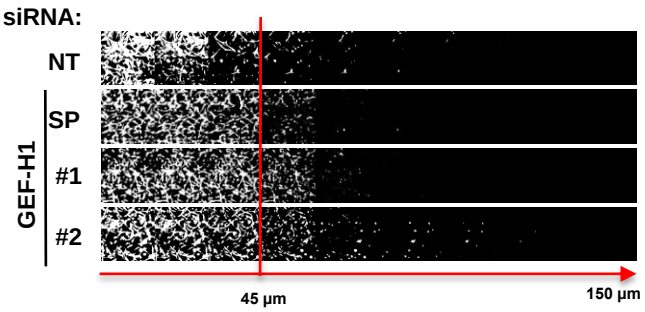

Figure 5B

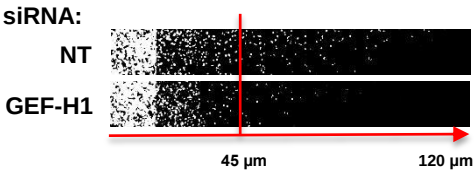

Figure 5D

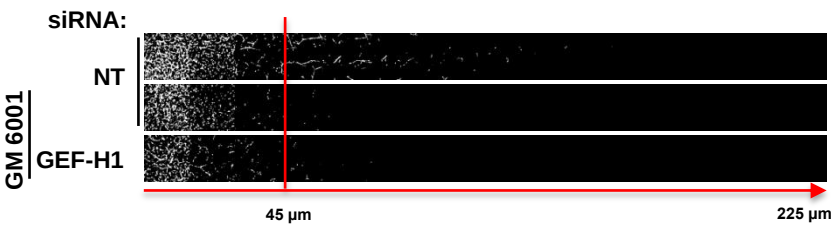

von Thun Fig. S4

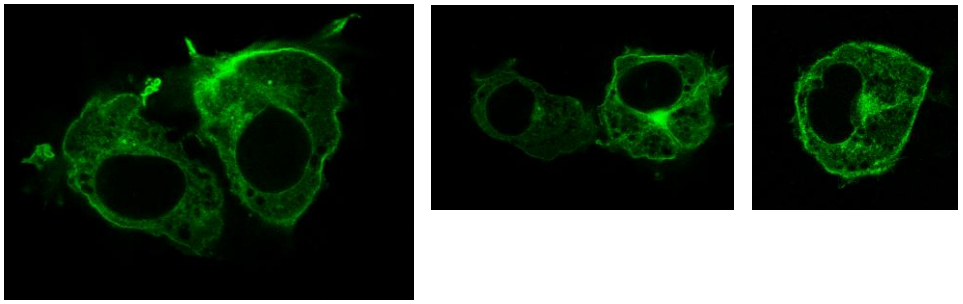

GEF-H1 WT +DMSO

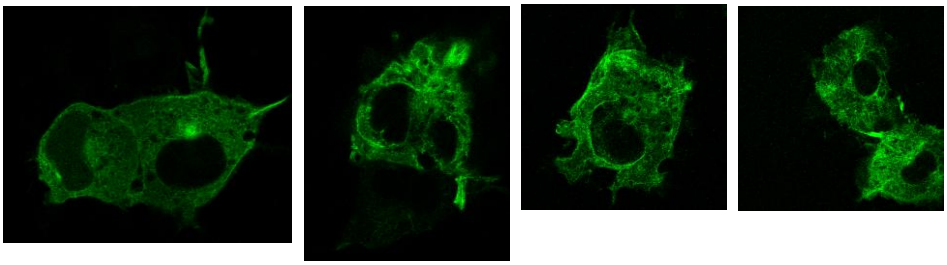

GEF-H1 WT +10μM U0126

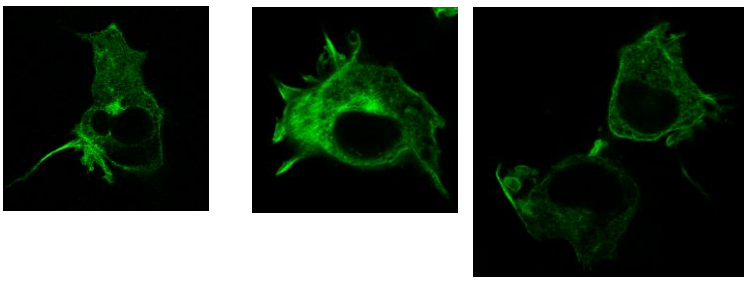

GEF-H1 S-A +DMSO

von Thun Fig. S5

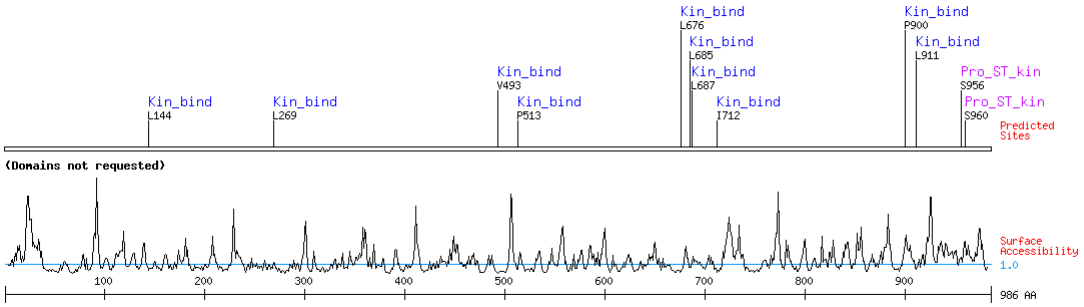

Proline-dependent serine/threonine kinase group (Pro_ST_kin)

Erk1 Kinase — Gene Card **MAPK3**

Site	Score	Percentile	Sequence	SA
S956	0.4647	0.229 %	EEGSSRLSPPHSPRD	1.614

Erk1 Kinase — Gene Card **MAPK3**

Site	Score	Percentile	Sequence	SA
S960	0.5032	0.481 %	SRLSPPHSPRDFTRM	3.268

Kinase binding site group (Kin_bind)

Erk1 Binding — Gene Card **MAPK3**

Site	Score	Percentile	Sequence	SA
P513	0.3288	0.200 %	KDQKVIEPTLDKPSV	0.428

Erk D-domain — Gene Card **MAPK1**

Site	Score	Percentile	Sequence	SA
L687	0.5684	0.149 %	PREPALPLEPDSGGN	1.078

Erk D-domain — Gene Card **MAPK1**

Site	Score	Percentile	Sequence	SA
L269	0.6049	0.279 %	RTGMLEELHLEPGVV	1.102

Erk D-domain — Gene Card **MAPK1**

Site	Score	Percentile	Sequence	SA
V493	0.6200	0.351 %	GRFKDVLVLLMTDVL	0.070

Erk D-domain — Gene Card **MAPK1**

Site	Score	Percentile	Sequence	SA
L144	0.6380	0.471 %	SRRGRSSLSLAKSVS	0.379

Erk D-domain — Gene Card **MAPK1**

Site	Score	Percentile	Sequence	SA
L676	0.6474	0.543 %	LVGPGVELLLTPREP	0.238

Erk D-domain — Gene Card **MAPK1**

Site	Score	Percentile	Sequence	SA
I712	0.6607	0.676 %	ARTFNGSIELCRADS	0.163

Erk D-domain — Gene Card **MAPK1**

Site	Score	Percentile	Sequence	SA
L685	0.6701	0.785 %	LTPREPALPLEPDSG	0.652

Erk1 Binding — Gene Card **MAPK3**

Site	Score	Percentile	Sequence	SA
P900	0.7015	0.959 %	LYLSFNPPQPSRGTD	3.284

Erk D-domain — Gene Card **MAPK1**

Site	Score	Percentile	Sequence	SA
L911	0.5991	0.252 %	RGTDRLDLPVTTRSV	0.431